# Quantifying the Magnitude of Pharyngeal Obstruction During Sleep Using Airflow Shape

Dwayne L Mann, Philip I Terrill, Ali Azarbarzin, Sara Mariani, Angelo Franciosini, Alessandra Camassa, Thomas Georgeson, Melania Marques, Luigi Taranto-Montemurro, Ludovico Messineo, Susan Redline, Andrew Wellman, Scott A Sands.

# Online Data Supplement

# Simulation illustrating the relationship between airflow obstruction and flow shape
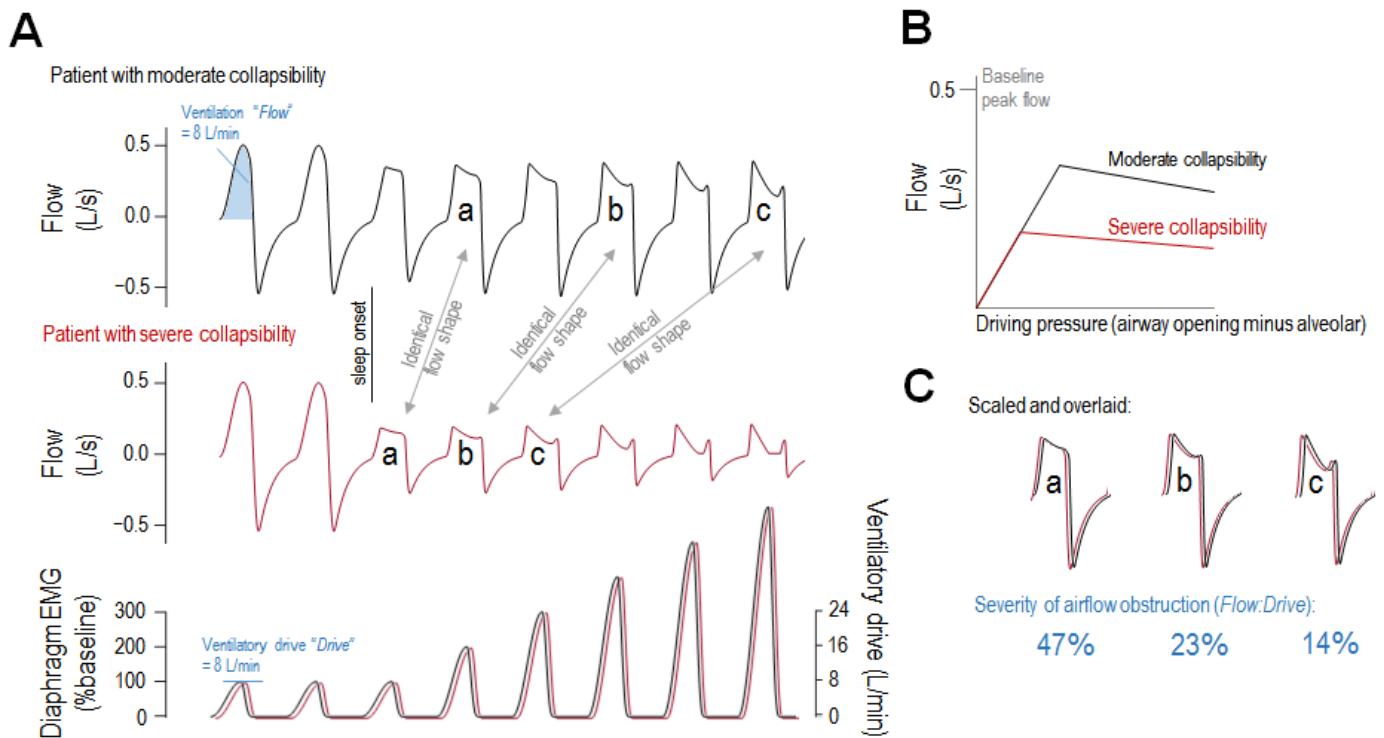


**Figure S1: The flow-time profile ("flow shape") is theoretically a manifestation of the degree of mismatch between the actual ventilatory *flow* and the intended airflow or ventilatory *drive*, i.e. *flow*:*drive*.** (A) Two computer simulations are presented. In both "patients", the same progressive rise in ventilatory drive was provided (diaphragm EMG). The "patient" with moderate collapsibility (black, top) has an airway that permits twice the airflow of the "patient" with severe collapsibility (red, middle), see airway flow-pressure profile in Panel B. Note that a more collapsible airway (black vs red) and increased ventilatory drive both promote more apparent flow limitation (flattening and scooping of inspiratory flow, elongation of inspiratory time). Note that the exact same flow shape occurs whenever moderate collapse is exposed to twice that of the severe collapse (flow shapes "a", "b", "c"). In each case of identical shape, there has been no change in the ratio of ventilation to ventilatory drive (*flow*:*drive* = 47% in "a", 23% in "b", 14% in "c"), hence no change in manifest flow shape, see Panel C for scaled and overlaid signals.

Model details pertaining to Figure S1 are as follows: The equation of motion of the respiratory system was a standard lumped resistance and compliance model, modified to include a nonlinear resistance consistent with flow-limitation (see Panel B); respiratory system compliance = 80 ml/cmH$_2$O, resistance (linear portion at low flow) was based on a time constant of 0.6 s, peak inspiratory muscle pressure (shown as "diaphragm EMG") was 8 cmH$_2$O at baseline. A short time-constant for pharyngeal collapse (30 ms) was incorporated to mimic physiological signals. Greater collapsibility was simulated by reducing the maximum inspiratory flow while maintaining the shape of the pressure-flow profile constant.

**Calibration of diaphragm EMG to measure ventilatory drive**

To calibrate intraesophageal diaphragm EMG swings (EMGdi, units of μV) to reflect *intended ventilation* or *ventilatory drive* (units of L/min) i.e. the ventilation expected based on neural output when the respiratory mechanics are normal for each individual, we identified suitable reference breaths throughout the night as follows: Breaths during wake or arousal (at least two breaths away from scored sleep) were selected. Breaths were excluded if they were within the margins of a scored respiratory event or had a reduced ventilation (more than 30% below local average). We expected that *ventilation* and *ventilatory drive* were equal at these times. The use of wakefulness levels to calibrate drive and define normal respiratory mechanics means that any baseline non-sleep-related mechanical deficits can be avoided in the measurement, i.e. only a sleep-related mismatch between flow and drive will be captured by our gold standard.

For each breath, we calculated the ratio of the ventilation ($V_E$) to EMGdi (root-mean-squared diaphragm EMG signal, 160 ms smoothing; EMG swings (in μV) were taken as the peak minus pre-inspiratory values, and normalised to yield values in L/min using automatically-identified reference breaths defined above), given by $G=V_E$:EMGdi (units of L/min/μV). Rather than define a single average value of G for calibration of diaphragm EMG, we considered that in some circumstances the diaphragm EMG signal amplitude may change over time. Thus, a moving-time average of G was calculated to handle possible overnight calibration drift; a weighting approach allowed the moving-time-averaged calibration factor to be determined predominantly by local calibration data where available. EMGdi for each breath was multiplied by G to yield *ventilatory drive* (units of L/min).

**Nasal pressure linearisation**

The nasal pressure signal was linearised using a power-law transform. Traditionally, nasal pressure has been linearised to correspond more closely with relative changes in (gold-standard) pneumotachograph flow using an "exponent" of ½, i.e. the square-root transform [1-3]. However, it is evident from the original data, that the square-root transformation is an excessive approximation [1, 2]. In our recent studies, we instead advocated using a transform that was more subtle (i.e. power of ⅔) to obtain a closer match to data from the pneumotachograph ventilation signal [4, 5].

In the current study we measured gold-standard oronasal pneumotachograph flow and nasal pressure in 17 patients simultaneously, via a modified cannula referenced to mask pressure to reflect the clinically-available intranasal pressure signal; DC-coupled. Individual breaths were identified and segmented by an automated computer algorithm. Here we formally assessed several nasal pressure transforms: ½ (square-root), ⅔, ¾, and 1 (untransformed) and compared magnitude of ventilation (tidal volume × respiratory rate) on each breath (normalised to the local average) to gold standard values. Data from all patients were pooled. Results are

shown in Figure S2. We found that linearisation was best with ⅔ exponent, illustrated by greater symmetry around the line of identity; this exponent no longer led to the systematic overestimation of large breaths and underestimation of small breaths like the untransformed signal (Figure S2D), but also did not yield systematic *under*estimation of large breaths and *over*estimation of small breaths as with the square-root transform (Figure S2A).
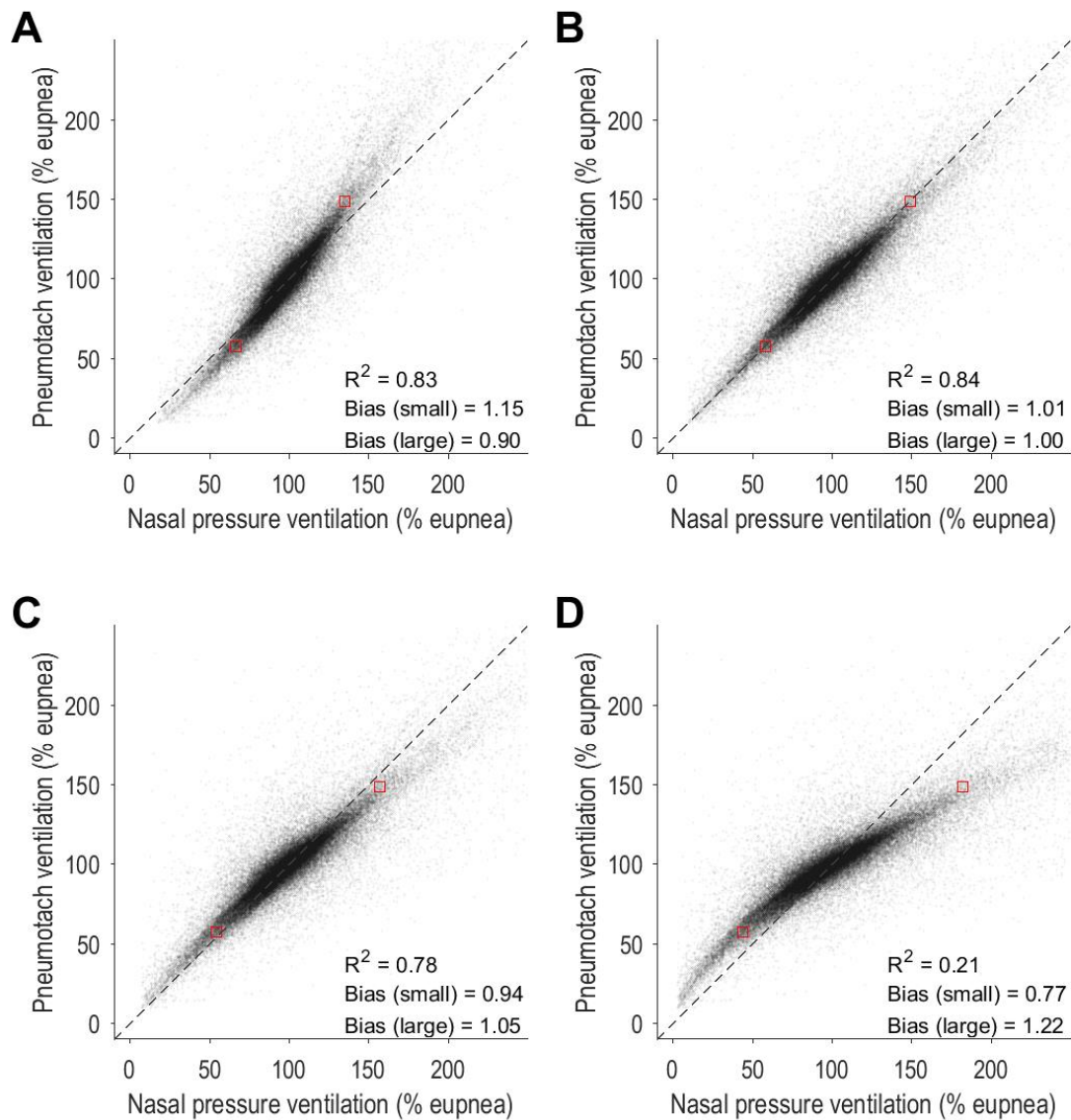


**Figure S2.** Nasal pressure transforms for clinical estimation of ventilation. Gold standard breath-by-breath ventilation in 17 patients (normalised to eupnoea i.e. local average in 3 min period) is compared to values estimated using nasal pressure. Values of 1 denote eupneic (average) ventilation. Transforms using the following exponents are shown **(A)** ½ (square-root), **(B)** ⅔, **(C)** ¾, and **(D)** 1 (untransformed). Note the improved symmetry about the line of identity (as shown by dashed line) with the ⅔ transform in **(B)**. The small red squares are shown to illustrate systematic discrepancies between measures (or lack thereof); median values are shown for large (>1.3×eupnoea) and small (<0.7×eupnoea) breaths. Note the systematic overestimation of small breaths (bias >1, where bias = nasal pressure ventilation / pneumotach ventilation), and underestimation of large breaths (bias<1) in panel A, with the traditional square root transform. $R^2$ = coefficient of determination.

**Initial feature list**

We identified 85 features from the literature and our own development that met the following criteria:

- Features represented shape aspects of pharyngeal airflow obstruction or flow limitation including: flattening, asymmetry, scooping, altered ratios of inspiratory/expiratory durations and volumes, irregularities, fluttering.

- Features were *breath independent*, i.e. stand-alone values could be obtained from a single breath without context, and do not rely on differences with respect to neighbouring breaths or selected reference breaths in the same individual. Thus we did not include features such as the change in inspiratory time relative to normal reference breaths [6].

- Features were *amplitude independent*, i.e. a breath that was simply larger but had the same shape would yield the same exact features, thereby enabling application in cases of un-calibrated flow signals.

- Features were *timing independent*, i.e. a breath that was simply slower and longer would yield the same features, thereby having equal potential application in cases where breathing is faster e.g. children. Accordingly, features from the "Asymmetry" and "Flutter" categories used uniform time spacing, to ensure timing independence. The time series for each inspiratory breath was resampled to 200 data points, while the time series for each expiratory breath was resampled to 250 data points prior to determination of feature values.

- Features consistently yield real values, i.e. yield "indeterminant" values <0.1% of the time.

- Features can be easily and rapidly computed without comparison to a template, lookup table, database, neural network or otherwise.

At the outset of the current investigation, we recognised that detection of appropriate inspiratory and expiratory start and end times could play a major role in determining values from each feature. Two approaches were employed: 1) our "original" in-house algorithm for detecting start and end times of breaths based primarily on volume maxima and minima, and 2) a modified timing algorithm that separately identifies the start and end times of inspiration and expiration based on the periods where 95% of the volume inspired/expired is observed, referred to as "transition" timing [7]. Based on preliminary univariate analysis indicating non-linear relationships, transformed features (square and square-root) were included as additional candidate features for selection.

# Table S1. List of 85 flow-shape features used throughout the study

| No. | Feature Label | Description | Ref. | Bivariate ($R^2$) vs. *flow:drive* | | *Pnasal vs. Pneumotach.* $R^2$ (bias) |
|-----|---------------|-------------|------|-----------------|--------|---------------------------|
| | | | | *Pneumotach.* | Pnasal | |
| **Flattening (N=28)** | | | | | | |
| 1 | MIF_PIF | mean Insp Flow/Peak Insp Flow | ¶[8, 9] | 0.46 [O, 2] | 0.31 | 0.73 (0.96) |
| 2 | Ali_InspFlat | AUC of abs(Insp Flow(Insp Time(0.1 to 0.9)) - MIF) | ¶[9, 10] | (-) 0.29 [T, 2] | 0.25 | 0.65 (1.01) |
| 3 | Ali_ExpFlat | AUC of abs(Exp Flow(Exp Time(0.2 to 0.8)) - MEF) | ¶[9, 10] | 0.28 [T, 1/2] | 0.23 | 0.6 (0.99) |
| 4 | Ali_InspExpFlat | Insp flat index / Exp flat index | [9] | (-) 0.3 [T, 1/2] | 0.23 | 0.32 (1.01) |
| 5 | AA_InspFlat9020 | sum(Insp Flow>0.9)/sum(Insp Flow>0.2); | [11] | 0.4 [O, 1/2] | 0.30 | 0.68 (0.96) |
| 6 | AA_InspFlat8020 | sum(Insp Flow>0.8)/sum(Insp Flow>0.2); | [11] | 0.42 [O, 1] | 0.30 | 0.72 (0.97) |
| 7 | AA_InspFlat7020 | sum(Insp Flow>0.7)/sum(Insp Flow>0.2); | [11] | 0.42 [O, 2] | 0.30 | 0.73 (0.96) |
| 8 | AA_InspFlat6020 | sum(Insp Flow>0.6)/sum(Insp Flow>0.2); | [11] | 0.42 [O, 2] | 0.31 | 0.71 (0.98) |
| 9 | AA_InspFlat5020 | sum(Insp Flow>0.5)/sum(Insp Flow>0.2); | [11] | 0.41 [O, 2] | 0.30 | 0.65 (0.98) |
| 10 | AA_InspFlat90Ti | sum(Insp Flow>0.9)/sum(Insp Flow>0); | [11] | 0.42 [O, 1/2] | 0.30 | 0.68 (0.96) |
| 11 | AA_InspFlat80Ti | sum(Insp Flow>0.8)/sum(Insp Flow>0); | [11] | 0.43 [O, 1] | 0.30 | 0.73 (0.97) |
| 12 | AA_InspFlat70Ti | sum(Insp Flow>0.7)/sum(Insp Flow>0); | [11] | 0.43 [O, 1] | 0.30 | 0.73 (0.98) |
| 13 | AA_InspFlat60Ti | sum(Insp Flow>0.6)/sum(Insp Flow>0); | [11] | 0.44 [O, 2] | 0.31 | 0.73 (0.97) |
| 14 | AA_InspFlat50Ti | sum(Insp Flow>0.5)/sum(Insp Flow>0); | [11] | 0.43 [O, 2] | 0.30 | 0.69 (0.98) |
| 15 | AA_ExpFlat9020 | sum(Exp Flow>0.9)/sum(Exp Flow>0.2); | [11] | 0.34 [O, 1] | 0.24 | 0.49 (0.95) |
| 16 | AA_ExpFlat8020 | sum(Exp Flow>0.8)/sum(Exp Flow>0.2); | [11] | 0.35 [O, 1] | 0.25 | 0.49 (0.99) |
| 17 | AA_ExpFlat7020 | sum(Exp Flow>0.7)/sum(Exp Flow>0.2); | [11] | 0.34 [O, 1] | 0.26 | 0.5 (1) |
| 18 | AA_ExpFlat6020 | sum(Exp Flow>0.6)/sum(Exp Flow>0.2); | [11] | 0.33 [O, 1] | 0.26 | 0.52 (1.01) |
| 19 | AA_ExpFlat5020 | sum(Exp Flow>0.5)/sum(Exp Flow>0.2); | [11] | 0.33 [T, 2] | 0.24 | 0.36 (1) |
| 20 | AA_ExpFlat90Te | sum(Exp Flow>0.9)/sum(Exp Flow>0); | [11] | 0.35 [O, 1/2] | 0.24 | 0.55 (0.98) |
| 21 | AA_ExpFlat80Te | sum(Exp Flow>0.8)/sum(Exp Flow>0); | [11] | 0.35 [O, 1/2] | 0.25 | 0.59 (1) |
| 22 | AA_ExpFlat70Te | sum(Exp Flow>0.7)/sum(Exp Flow>0); | [11] | 0.35 [T, 2] | 0.24 | 0.56 (0.98) |
| 23 | AA_ExpFlat60Te | sum(Exp Flow>0.6)/sum(Exp Flow>0); | [11] | 0.35 [T, 2] | 0.24 | 0.55 (0.99) |
| 24 | AA_ExpFlat50Te | sum(Exp Flow>0.5)/sum(Exp Flow>0); | [11] | 0.35 [T, 2] | 0.24 | 0.54 (1) |
| 25 | MIF50 | mean(Insp Flow(time(0.25 to 0.75))) | ¶[10, 12] | 0.48 [O, 2] | 0.33 | 0.83 (0.98) |
| 26 | MEF50 | mean(Exp Flow(time(0.25 to 0.75))) | ¶[10, 12] | (-) 0.32 [T, 1/2] | 0.23 | 0.49 (1.02) |
| 27 | Teschler | AUC btw y=1 and mean normalised flow (time(0.25:0.75)) | [10] | (-) 0.34 [T, 1] | 0.26 | 0.66 (1.02) |
| 28 | MostPromPeakW | Duration of Most Prominent Insp Peak / Ti. See Matlab "findpeaks" for details. | New | 0.48 [O, 1] | 0.35 | 0.7 (0.96) |
| **Scooping (deviation away from normal round contour) (N=8)** | | | | | | |
| 29 | AA_NED | (PIF - Flow at mid-Inspiration) / PIF | [13] | (-) 0.42 [O, 1/2] | 0.29 | 0.74 (1.04) |
| 30 | AreaUnderPeaksI | AUC between flow and connected peaks | New | (-) 0.49 [O, 1/2] | 0.35 | 0.76 (1.12) |
| 31 | QuadI | Absolute AUC between a quadratic best fit to 3 points in inspiration (x,y: start insp, 0; Ti/2, 1; end insp, Ti) and actual inspiratory waveform, divided by Ti. | [14] | (-) 0.46 [O, 1/2] | 0.31 | 0.82 (1.02) |
| 32 | QuadI50 | Same as SinI but AUC from 25th to 75th centiles of inspiratory time, divided by Ti | [12] | (-) 0.46 [O, 1/2] | 0.31 | 0.82 (1.02) |
| 33 | QuadE | Same as SinI but during expiration | New | (-) 0.33 [O, 1/2] | 0.30 | 0.77 (1) |
| 34 | InvParabI | Absolute AUC between an inverted parabola (with matched peak flow [value=1] forced to be zero at the start and end of inspiration) and inspiratory waveform, divided by Ti: Fit equation is y=c×((1-(x.^2)/(N/2)^2)); c is maximum | New | (-) 0.45 [O, 1/2] | 0.33 | 0.78 (1) |

| | | inspiratory flow (equal to 1), N is the length of the inspiratory flow, x is the adjusted time base, shifted to be equal about zero. | | | | |
|---|---|---|---|---|---|---|
| 35 | EllipseI | Same as InvParabI but using an ellipse fit to Inspiration: y=c×(((1-(x.^2)/(N/2)^2)).^(1/2)) | New | (-) 0.49  [O, 1/2] | 0.35 | 0.78  (1.03) |
| 36 | HypcosI | Same as InvParabI but using hyperbolic cosine fit to Inspiration, y=c×((1-cosh((x/(N/2)) × log(1+b+sqrt(2+b)×sqrt(b)))+b)/b); b is set as a constant = 10. | New | (-) 0.49  [O, 1/2] | 0.36 | 0.8  (1.02) |
| **Asymmetry (N=9)** | | | | | | |
| 37 | AsymIndex † | Expiratory flow limitation algorithm based on asymmetry | [15] | (-) 0.32  [O, 2] | 0.23 | 0.61  (1.04) |
| 38 | SkewDistInsp * § | skewness(distribution data of Insp flow) | ¶[16] | 0.27  [T, 1/2] | 0.24 | 0.82  (1.01) |
| 39 | KurtDistInsp * § | kurtosis(distribution data of Insp flow) | ¶[14] | (-) 0.3  [T, 1] | 0.24 | 0.44  (1) |
| 40 | SkewDistExp * § | skewness(distribution data of Exp flow) | ¶[16] | (-) 0.3  [T, 1] | 0.24 | 0.54  (0.91) |
| 41 | KurtDistExp * § | kurtosis(distribution data of Exp flow) | ¶[14] | (-) 0.28  [T, 1/2] | 0.23 | 0.25  (0.96) |
| 42 | AsymmetryInsp * | (areaL/AreaInsp Flow)-(areaR/AreaInsp Flow) | [11] | 0.27  [O, 2] | 0.24 | 0.6  (1) |
| 43 | KurtDataInsp * | kurtosis(Insp Flow); | [11] | 0.27  [O, 1/2] | 0.23 | 0.66  (0.96) |
| 44 | AsymmetryExp * | (areaL/AreaExp Flow)-(areaR/AreaExp Flow) | [11] | (-) 0.29  [T, 2] | 0.24 | 0.51  (0.73) |
| 45 | KurtDataExp * | kurtosis(Exp Flow) | [11] | (-) 0.31  [T, 1/2] | 0.23 | 0.42  (1.01) |
| **Timing and volume ratio measures (N=28)** | | | | | | |
| 46 | Ti_Ttot | Ti / (Ti+Te) | [8, 17] | (-) 0.32  [O, 2] | 0.28 | 0.7  (1.04) |
| 47 | Ti_Te | Ti / Te | [18] | (-) 0.32  [T, 1] | 0.28 | 0.62  (1.04) |
| 48 | TTran_i_Ti ‡ | Transition time (Insp to Exp) / Ti | [7] | 0.27  [T, 1/2] | 0.28 | 0.66  (1.03) |
| 49 | TTran_i_Ttot ‡ | Transition time (Insp to Exp) / Ttot | [7] | 0.27  [T, 1/2] | 0.26 | 0.69  (1.04) |
| 50 | TTran_e_Te ‡ | Transition time (Exp to Insp) / Te | [7] | (-) 0.29  [T, 1/2] | 0.25 | 0.45  (0.95) |
| 51 | TTran_e_Ttot ‡ | Transition time (Exp to Insp) / Ttot | [7] | (-) 0.27  [T, 1] | 0.23 | 0.56  (0.89) |
| 52 | VTi_VTe | VTi / VTe | [9] | (-) 0.3  [T, 1] | 0.23 | 0.15  (0.99) |
| 53 | VTi_VT | VTi / VT where VT = (VTi×Ti+VTe×Te) / (Ti + Te) | [9] | (-) 0.3  [T, 1] | 0.23 | 0.15  (0.99) |
| 54 | VTe_VT | VTe / VT where VT = (VTi×Ti+VTe×Te) / (Ti + Te) | [9] | 0.28  [T, 1/2] | 0.23 | 0.33  (1) |
| 55 | VPEF/VTe | Volume at PEF / VTe | [19, 20] | 0.27  [T, 2] | 0.23 | 0.14  (1.1) |
| 56 | VPIFVTi | Insp Volume at PIF / VTi | ¶[21] | (-) 0.27  [O, 2] | 0.23 | 0.67  (1.01) |
| 57 | InspVol_03Ti | Insp Volume at ⅓ × Ti | ¶[21] | (-) 0.27  [T, 2] | 0.23 | 0.71  (0.98) |
| 58 | PIF_MIF | Peak Insp flow / Mean Insp flow | [16] | (-) 0.41  [O, 1/2] | 0.30 | 0.72  (1.01) |
| 59 | FTi | Inspiratory fall time, 90% to 10% (of PIF) / Ti | ¶[22] | (-) 0.28  [O, 2] | 0.23 | 0.69  (1.11) |
| 60 | RTi | Inspiratory rise time, 10% to 90% (of PIF) / Ti | ¶[22] | (-) 0.3  [O, 2] | 0.26 | 0.67  (1.2) |
| 61 | DTi | Inspiratory dwell time, flow >= 90% (of PIF) / Ti | ¶[22] | 0.37  [O, 1/2] | 0.27 | 0.55  (0.97) |
| 62 | FTe | Expiratory fall time, 90% to 10% (of PEF) / Te | [22] | (-) 0.31  [O, 2] | 0.26 | 0.47  (1.02) |
| 63 | RTe | Expiratory rise time, 10% to 90% (of PEF) / Te | [22] | 0.3  [T, 1/2] | 0.25 | 0.57  (1) |
| 64 | DTe | Expiratory dwell time, flow >= 90% (of PEF) Te | [22] | 0.33  [O, 1/2] | 0.24 | 0.57  (1) |
| 65 | PIF_PEF | Peak Insp flow / Peak Exp flow | [16, 23] | (-) 0.28  [O, 1/2] | 0.27 | 0.62  (0.97) |
| 66 | MIF_MEF | mean Insp flow to mean Exp flow | ¶[16] | (-) 0.32  [O, 1/2] | 0.28 | 0.64  (0.96) |
| 67 | MIF50_MEF50 | mean (Insp Flow(time(0.25 to 0.75))) / same in Exp | ¶(17) | (-) 0.28  [O, 1/2] | 0.24 | 0.64  (0.96) |
| 68 | SeriesIEflow | ratio of Insp flow to Exp flow at mid volumes | [24] | (-) 0.27  [T, 1] | 0.23 | 0.13  (1.03) |
| 69 | SeriesIEtime | ratio of Insp time to Exp time at mid volumes | ¶[24] | (-) 0.36  [T, 1] | 0.32 | 0.55  (0.97) |
| 70 | KaplanIEvol | ratio of Insp volume to Exp volume at mid times | ¶[24] | 0.27  [T, 2] | 0.23 | 0.14  (1.1) |
| 71 | TpeakI_Ti | Time to PIF / Ti | ¶[25] | (-) 0.27  [O, 2] | 0.24 | 0.72  (1) |
| 72 | TpeakE_Te | Time to PEF / Te | [19, 25, 26] | 0.32  [T, 1/2] | 0.26 | 0.59  (1.01) |

| 73 | TpeakI_TpeakE | Time to PIF / time to PEF | ¶(17) | (-) 0.33 [O, 1/2] | 0.28 | 0.61 (1.01) |
|---|---|---|---|---|---|---|
| **Fluttering (N=12)** | | | | | | |
| 74 | Power5to12I * | power in Insp flutter [5 to (Fs/2) Hz]/ PIF squared | [9] | (-) 0.47 [O, 1/2] | 0.42 | 0.6 (1.02) |
| 75 | Power5to12E * | power in Exp flutter [5 to (Fs/2) Hz]/ PEF squared | [9] | (-) 0.31 [O, 1/2] | 0.26 | 0.54 (1.04) |
| 76 | InspExpFlutPowOrig * | power in Insp flutter / power in Exp flutter [5 to (Fs/2)] | ¶[9] | (-) 0.3 [O, 2] | 0.24 | 0.46 (0.83) |
| 77 | InspExpFlutPowOrig_Sum * | power in Insp / (Pow Insp + Pow Exp) | ¶[9] | (-) 0.3 [O, 2] | 0.24 | 0.46 (0.83) |
| 78 | InspFlutPow4to7 * | power in Insp flutter [4-7 Hz]  / PIF squared | ¶[9] | (-) 0.34 [O, 1/2] | 0.29 | 0.57 (0.95) |
| 79 | ExpFlutPow4to7 * | power in Exp flutter [4-7 Hz] / PEF squared | ¶[9] | (-) 0.31 [T, 1/2] | 0.24 | 0.49 (1.01) |
| 80 | InspExpFlutPow4to7 * | power in Insp flutter / power in Exp flutter [4-7 Hz] | ¶[9] | 0.28 [O, 1/2] | 0.25 | 0.58 (0.97) |
| 81 | InspExpFlutPow4to7_Sum * | power in Insp flutter / (pow in Insp + pow in Exp [4-7 Hz]) | ¶[9] | 0.28 [O, 1/2] | 0.25 | 0.58 (0.97) |
| 82 | InspFlutPow8to12 * | power in Insp flutter [8-12 Hz] / PIF squared | ¶[9] | (-) 0.43 [O, 1/2] | 0.40 | 0.57 (0.92) |
| 83 | ExpFlutPow8to12 * | power in Exp flutter [8-12 Hz] / PEF squared | ¶[9] | (-) 0.31 [T, 1/2] | 0.24 | 0.53 (0.85) |
| 84 | InspExpFlutPow8to12 * | power in Insp flutter / power in Exp flutter [8-12 Hz] | ¶[9] | (-) 0.29 [O, 1] | 0.23 | 0.2 (0.9) |
| 85 | InspExpFlutPow8to12_Sum * | power in Insp flutter / (pow in Insp + pow in Exp [8-12 Hz]) | ¶[9] | (-) 0.28 [O, 2] | 0.23 | 0.36 (0.91) |

Bivariate results are not cross-validated, showing timing variant as O (original) or transition (T) and transform (1/2, 1 or 2) for highest coefficient of determination for pneumotachogragh (Pneumotach.) derived feature value vs *flow:drive*. Transform and timing variant held for nasal pressure (Pnasal) derived feature value vs *flow:drive*. The sign of the corresponding correlation coefficient is presented as prefix (-) if negative. Bias is nasal pressure feature value / pneumotach feature value. AUC = Area Under Curve. Ti = Inspiratory Time. Te = Expiratory Time. Insp = Inspiration. Exp = Expiration. PIF = Peak Inspiratory Flow. PEF = Peak Expiratory Flow. MIF = Mean Inspiratory Flow. MEF = Mean Expiratory Flow. btw = between. Ref = Reference. Fs = Sample Rate. Hz = Hertz. ¶Adapted based on cited reference. *Uses uniform length for timing. § Flow waveform shape preserved as a distribution. † Only original timing variant used during processing. ‡ Only transition timing variant used during processing.

## Feature reduction

*Removal of non-robust features.* We conducted a sensitivity analysis to ensure that the model presented is robust, and not subject to significant performance degradation due to subtle changes in input parameters. As demonstrated in Table S2, we observed no reduction in model performance when increasing the $R^2$ threshold for inclusion, up to 0.5. Further increases to the inclusion threshold resulted in a steady progressive reduction in performance using pneumotachograph, and a step static decline in performance using nasal pressure.

*Pre-screening with separate data.* In a preliminary implementation of this work (prior to the discovery of non-robust features) we used a feature pre-screening process with a separate dataset (see "Feature pre-screening with external data" below). However, we chose not to implement pre-screening for the final method based on the following: 1) The discovery of non-robust features (pneumotach versus nasal pressure) meant that pre-screening (before robustness was known) would remove robust features from the selection pool that would then be excluded later. 2) Pre-screening had negligible influence on the model performance but added complexity.

**Table S2. Sensitivity analysis**

| R² threshold for feature-term inclusion | Number of feature-terms in model | Performance using pneumotachograph ($R^2$) | Performance using nasal pressure ($R^2$) |
|---|---|---|---|
| 0 | 495 | 0.59 | 0.48 |
| ⅓ | 406 | 0.58 | 0.48 |
| ½ | 295 | 0.58 | 0.48 |
| ⅔ | 127 | 0.56 | 0.39 |
| ¾ | 44 | 0.54 | 0.39 |

Threshold for threshold for inclusion is the association (as coefficient of determination, $R^2$) between pneumotachograph derived feature-term and corresponding nasal pressure derived feature-term. The Number of feature-terms in model is the minimum number from each loop of the leave-one-out cross-validation. The results reported are breath level association for cross-validated multivariable model predicted *flow:drive* and gold-standard *flow:drive*. Results presented are cross-validated values.

**Multivariable linear regression to predict airflow obstruction**

As described in the main manuscript, multivariable linear regression with backwards elimination was used to model the relationships between shape features and airflow obstruction (continuous variable, ratio of *flow:drive*). Feature-terms with coefficient of determination $R^2 \leq 0.5$ between pneumotachograph derived feature and nasal pressure derived feature, were excluded from analysis. Figure S3 shows cross-validated testing performance increasing rapidly, while mean absolute error falls rapidly for the first three features. We observed a steady and progressive increase in performance with increasing feature number and model complexity, with performance plateauing by 30 features. We choose a value of 25 features as a sensible compromise between accuracy and complexity.

*Model weighting.* The regression was inversely weighted based on the number of breaths in each airflow obstruction class (normal: *flow:drive*>90%; mild: 70-90%, moderate: 50-70%; severe: 30-50%, very severe: <30%).
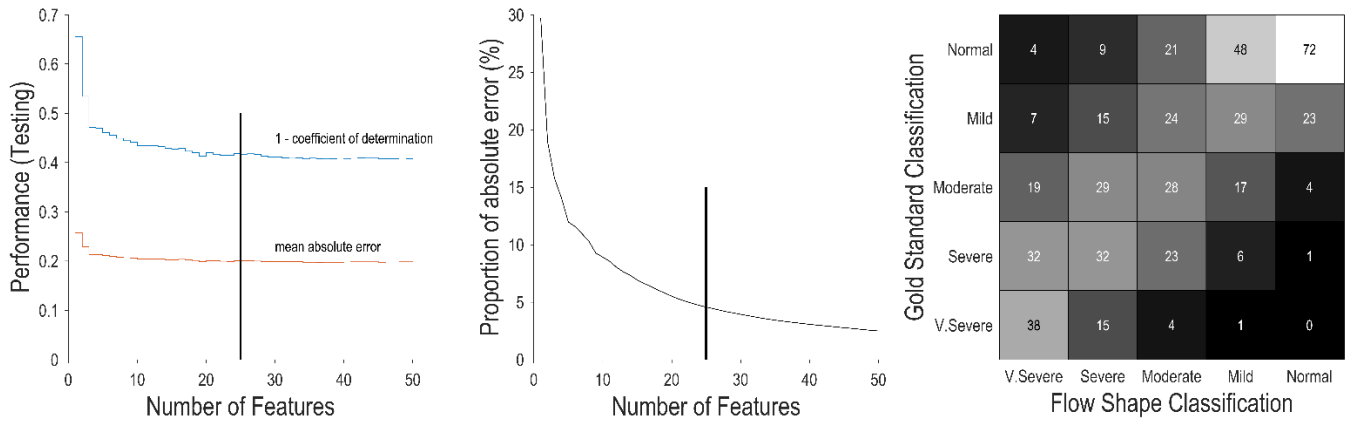
**Figure S3.** *Left.* Performance versus number of feature terms with pneumotachograph airflow. Performance (cross-validated) increased with each additional feature included. *Middle.* By 25 features (vertical bar), performance was at ~4.6% of the total error (at 100 feature-terms). *Right.* Predictive performance confusion matrix for each severity classification, with thresholds being >90% Normal, 70-90% Mild, 50-70% Moderate, 30-50% Severe, <30% Very Severe (V.Severe). Each column sums to 100%, and indicates the fraction of predicted breaths in each class that were correctly classified. On average, the classification prediction was exact in 39.7% of breaths, and within one severity class in 81.7% of breaths. Classification performance for individuals is provided in Table S4.

For consistency with our primary analysis with pneumotachograph flow, we used 25 features and the corresponding beta coefficients in our nasal pressure flow surrogate analysis. Similar to our primary results, we observed an initial rapid increase in performance, followed by varied increases in performance up to 25 features (Figure S4). In contrast to our primary analysis, we observed that performance continued to rise beyond 25 features, albeit very slowly. This may indicate that a model developed using nasal pressure signal requires a different number of features to train. We note that the results of this analysis could be improved simply by selecting the optimal number of features.
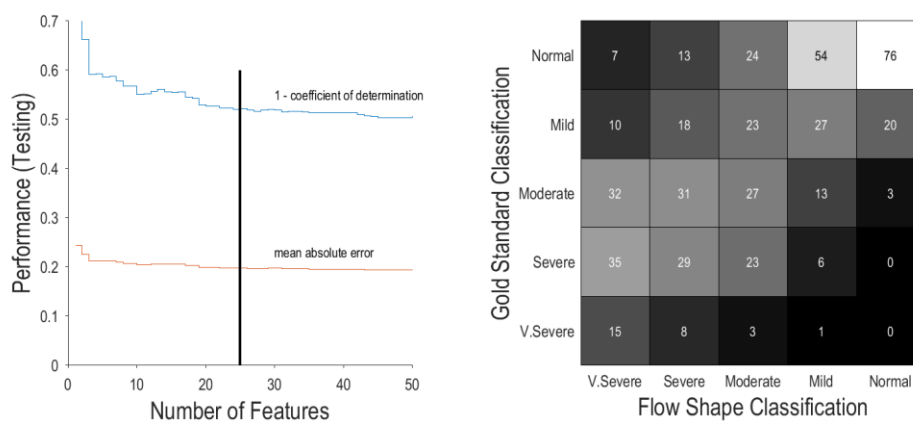


**Figure S4.** *Left:* Performance versus number of feature terms with transformed nasal pressure. Performance increased with each feature added, and continued to increase slowly beyond 25 features. *Right:* Predictive performance confusion matrix for each severity classification, with thresholds being >90% Normal, 70-90% Mild, 50-70% Moderate, 30-50% Severe, <30% Very Severe (V.Severe). Each column sums to 100%, and indicates the fraction of predicted breaths in each class that were correctly classified. On average, the classification prediction was exact in 34.8% of breaths, and within one severity class in 76.3% of breaths.

**Table S3. Multivariable linear regression model (25 features) to estimate airflow obstruction severity**

| Feature No. | Feature | Timing method | Transform | Multivariate β ± SE | Bivariate ($R^2$) Pneumo. feature vs *flow:drive* | Pneumo. feature vs Pnasal feature | Bias (Pnasal / Pneumo.) |
|---|---|---|---|---|---|---|---|
| | Intercept | | | -1.22 ± 0.04 | | | |
| 75 | Power5to12E | O | 1/2 | -1.88 ± 0.05 | (-) 0.31 | 0.54 | 1.04 |
| 74 | Power5to12I | O | 1/2 | -4.48 ± 0.09 | (-) 0.47 | 0.6 | 1.02 |
| 33 | QuadE | O | 1/2 | -0.70 ± 0.02 | (-) 0.33 | 0.77 | 1 |
| 32 | QuadI50 | O | 1/2 | 0.91 ± 0.02 | (-) 0.46 | 0.82 | 1.02 |
| 30 | AreaUnderPeaksI | O | 1/2 | -0.39 ± 0.01 | (-) 0.49 | 0.76 | 1.12 |
| 30 | AreaUnderPeaksI | O | 2 | 1.53 ± 0.04 | (-) 0.37 | 0.69 | 1.57 |
| 38 | SkewDistInsp | O | 1/2 | 0.12 ± 0.003 | 0.27 | 0.81 | 1.13 |
| 57 | InspVol_03Ti | O | 1 | -0.75 ± 0.02 | (-) 0.26 | 0.64 | 1 |
| 1 | MIF_PIF | O | 1 | 0.87 ± 0.01 | 0.45 | 0.74 | 0.98 |
| 33 | QuadE | O | 1 | 0.25 ± 0.01 | (-) 0.32 | 0.71 | 1 |
| 3 | Ali_ExpFlat | T | 1/2 | 0.98 ± 0.03 | 0.28 | 0.6 | 0.99 |
| 46 | Ti_Ttot | O | 1 | -3.44 ± 0.08 | (-) 0.31 | 0.72 | 1.02 |
| 46 | Ti_Ttot | O | 1/2 | 4.15 ± 0.10 | (-) 0.3 | 0.72 | 1.01 |
| 45 | KurtDataInsp | O | 1/2 | 0.26 ± 0.01 | 0.27 | 0.66 | 0.96 |
| 45 | KurtDataInsp | O | 1 | -0.043 ± 0.002 | 0.27 | 0.65 | 0.93 |
| 31 | QuadI | T | 1 | -0.42 ± 0.01 | (-) 0.43 | 0.81 | 1.01 |
| 3 | Ali_ExpFlat | T | 1 | -0.71 ± 0.02 | 0.27 | 0.63 | 0.98 |
| 21 | AA_ExpFlat80Te | O | 2 | 0.18 ± 0.01 | 0.34 | 0.56 | 0.99 |
| 74 | Power5to12I | T | 1 | 27.6 ± 0.69 | (-) 0.37 | 0.51 | 1.04 |
| 74 | Power5to12I | T | 1/2 | -3.28 ± 0.11 | (-) 0.42 | 0.65 | 1.02 |
| 44 | AsymmetryExp | T | 1 | -0.12 ± 0.005 | (-) 0.28 | 0.65 | 0.85 |
| 72 | TpeakE_Te | O | 1 | -0.43 ± 0.01 | 0.29 | 0.7 | 1.03 |
| 55 | VPEF_VTe | O | 1/2 | 0.45 ± 0.02 | 0.31 | 0.54 | 1 |
| 73 | TpeakI_TpeakE | T | 1/2 | 0.031 ± 0.001 | (-) 0.33 | 0.54 | 1.03 |
| 78 | InspFlutPow4to7 | O | 1/2 | 0.82 ± 0.05 | (-) 0.34 | 0.57 | 0.95 |

Features are in order of importance based on backwards feature elimination (i.e. Power5to12E was the final feature remaining after sequential elimination). Feature No. corresponds with Table S1. Timing method O and T denote "original" timing and "transition" timing methods for breath detection. Transform describes the exponent: ½ = square-root transformed, 1 = un-transformed, 2 = squared (note: only magnitudes were transformed i.e. negative values remained negative). β, the beta coefficient estimates. SE, standard error of the coefficient estimates. All terms were statistically significant contributors (note very small values of SE) with $P<1 \times 10^{-50}$. Bivariate performance is not cross-validated.

**Table S4. Cross-validated classification performance in individuals**

| Patient ID# | Pneumotachograph flow features | | Nasal pressure features | |
|---|---|---|---|---|
| | Exact Class % | Within One Class % | Exact Class % | Within One Class % |
| 1 | 57.7 | 94.8 | - | - |
| 2 | 40.2 | 82.1 | 45.4 | 90 |
| 3 | 47.1 | 85.3 | - | - |
| 4 | 37.3 | 83.3 | 34.6 | 82.1 |
| 5 | 37.5 | 73.9 | - | - |
| 6 | 37.3 | 72 | 30 | 68.1 |
| 7 | 30.1 | 72.3 | 29.2 | 69.3 |
| 8 | 38.4 | 76.4 | - | - |
| 9 | 23.1 | 52.5 | - | - |
| 10 | 52.4 | 92.1 | - | - |
| 11 | 46.2 | 88.5 | - | - |
| 12 | 35.8 | 75.9 | - | - |
| 13 | 40.8 | 81.9 | 40.1 | 83.7 |
| 14 | 30.7 | 64.8 | - | - |
| 15 | 55 | 94 | - | - |
| 16 | 54.7 | 95.5 | - | - |
| 17 | 34 | 79.7 | 35.5 | 78.5 |
| 18 | 28.5 | 60.1 | - | - |
| 19 | 43.9 | 81.8 | - | - |
| 20 | 45.9 | 85.1 | - | - |
| 21 | 42.6 | 84.8 | - | - |
| 22 | 36.3 | 79.2 | - | - |
| 23 | 35.8 | 75.7 | - | - |
| 24 | 48.8 | 86.9 | - | - |
| 25 | 42.5 | 82.4 | - | - |
| 26 | 43.7 | 89.2 | 40.2 | 81 |
| 27 | 49.2 | 90.8 | 41.9 | 84.8 |
| 28 | 36.4 | 81 | 25 | 54.6 |
| 29 | 23.7 | 68.6 | 27.9 | 68.5 |
| 30 | 34.9 | 76.8 | 36.2 | 78.2 |
| 31 | 30.1 | 79.3 | - | - |
| 32 | 39.9 | 76.6 | - | - |
| 33 | 33.6 | 73.5 | - | - |
| 34 | 46.5 | 86.9 | 39.3 | 77 |
| 35 | 37 | 75.8 | - | - |
| 36 | 37.5 | 82.2 | - | - |
| 37 | 43.6 | 83.9 | 42.3 | 83.2 |
| 38 | 39.1 | 80.2 | 29.1 | 66.6 |
| 39 | 42.6 | 82.4 | 35.8 | 74.6 |
| 40 | 42.9 | 84.6 | 44.8 | 84.4 |
| 41 | 30.8 | 58.1 | 28.3 | 56.1 |

Individual patient performance for categorisation into normal, mild, moderate, severe and very severe flow-limited classes using the pneumotachograph flow shape features. The "Exact Class %" column indicates the proportion of breaths that classified exactly, while the "Within One Class %" column shows the proportion of breaths that were correct, if accepting the adjacent class as correct. All values represent the percentage correctly classified using flow shape alone, assessed against gold-standard.

**Simplified 5-feature model**

Table S5 presents a simplified model for estimating *flow:drive* utilising only five feature-terms. While we observe a slight reduction in breath-level overall performance, it continues to perform remarkably well at the patient-level, in pneumotachograph derived feature-terms (see Figure S5). This reduced feature model performs adequately well in nasal pressure derived feature terms (see Figure S6).

The five features-terms in our simplified model quantified signal variability (spectral power) in inspiration and expiration respectively, the deviation from a normal rounded contour in inspiration and expiration respectively, and the magnitude of "scooping" between multiple inspiratory peaks (when present). The major role of expiratory shape abnormalities in our estimation of pharyngeal airflow obstruction (often referred to as "inspiratory flow limitation")—was unexpected, but is consistent with the increased expiratory resistance observed in some patients [15, 27, 28].

**Table S5. Multivariable linear regression model (5 features) to estimate airflow obstruction severity**

| Feature No. | Feature | Timing method | Transform | Multivariate |
|---|---|---|---|---|
| | | | | β ± SE |
| | Intercept | | | 1.3 ± 0.003 |
| 75 | Power5to12E | O | ½ | -2.32 ± 0.04 |
| 74 | Power5to12I | O | ½ | -4.17 ± 0.05 |
| 33 | QuadE | O | ½ | -0.24 ± 0.003 |
| 32 | QuadI50 | O | ½ | -0.68 ± 0.01 |
| 30 | AreaUnderPeaksI | O | ½ | -0.3 ± 0.01 |

Feature No. corresponds with Table S1. Timing method O and T denote "original" timing and "transition" timing methods for breath detection. Transform describes the exponent: ½ = square-root transformed, 1 = un-transformed, 2 = squared (note: only magnitudes were transformed i.e. negative values remained negative). β, the beta coefficient estimates. SE, standard error of the coefficient estimates.
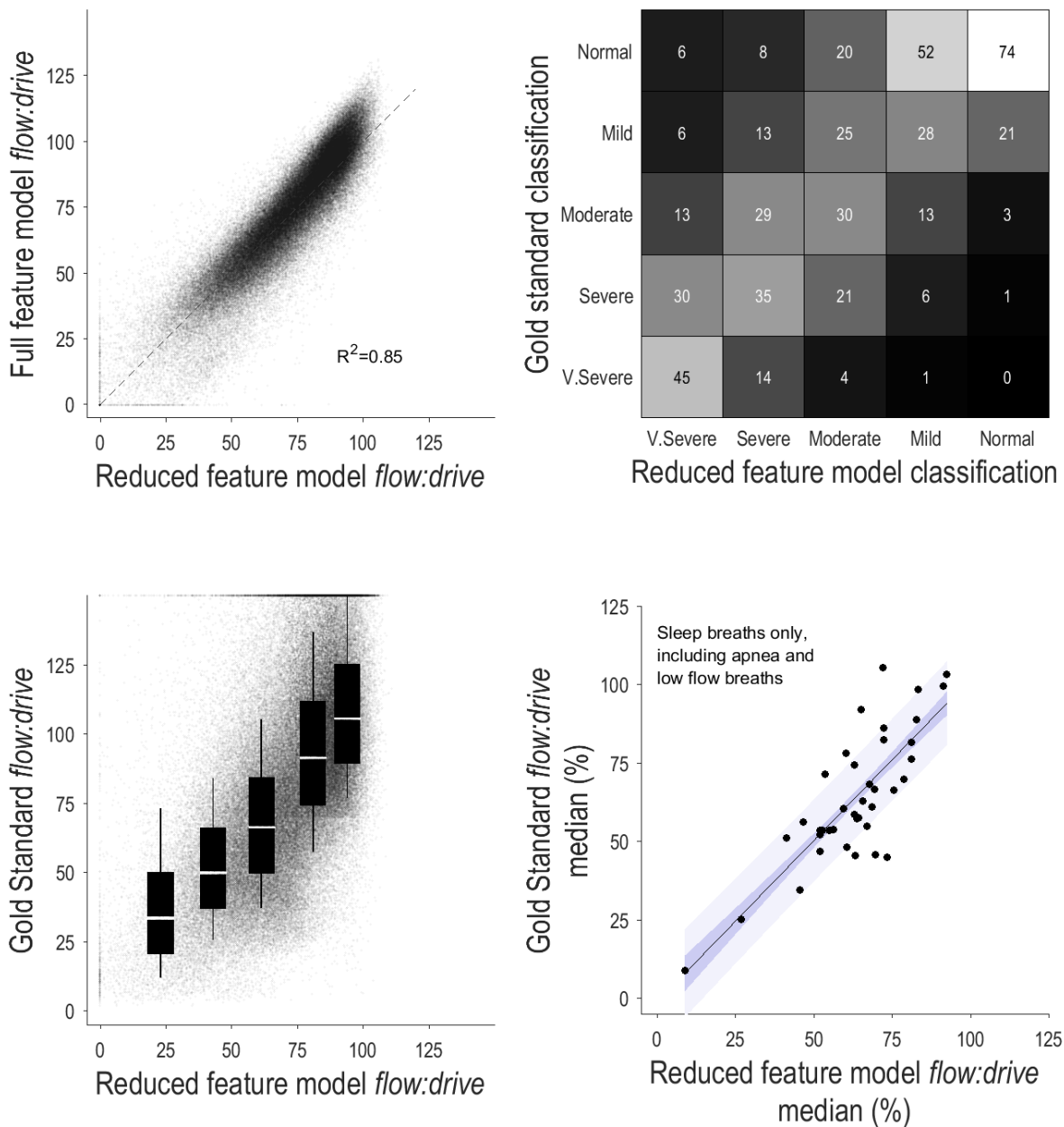
**Figure S5.** Reduced feature model performance, using *pneumotachograph flow features*. **(Top Left)** The association between the reduced feature model predicted *flow:drive* values and the full 25 feature model predicted *flow:drive* values is very high ($R^2$=0.85). **(Top Right)** Predictive performance confusion matrix for each severity classification, with thresholds being >90% Normal, 70-90% Mild, 50-70% Moderate, 30-50% Severe, <30% Very Severe (V.Severe). Each column sums to 100%, and indicates the fraction of predicted breaths in each class that were correctly classified. On average, the classification prediction was exact in 42.6% of breaths, and within one severity class in 83.8% of breaths. **(Bottom Left)** Scatter plot showing a strong association between reduced feature model predicted *flow:drive* and gold-standard *flow:drive* values. The box plot overlay shows summary statistics (box and central line show IQR and median respectively, whiskers show 10th and 90th percentiles) for breaths within each severity classification. **(Bottom Right)** Scatter plot showing the novel patient level metric, median *flow:drive* (during sleep, including apnoea breaths). A very strong association exists between reduced feature model predicted and gold-standard patient median *flow:drive* during sleep. ($R^2$, coefficient of determination)
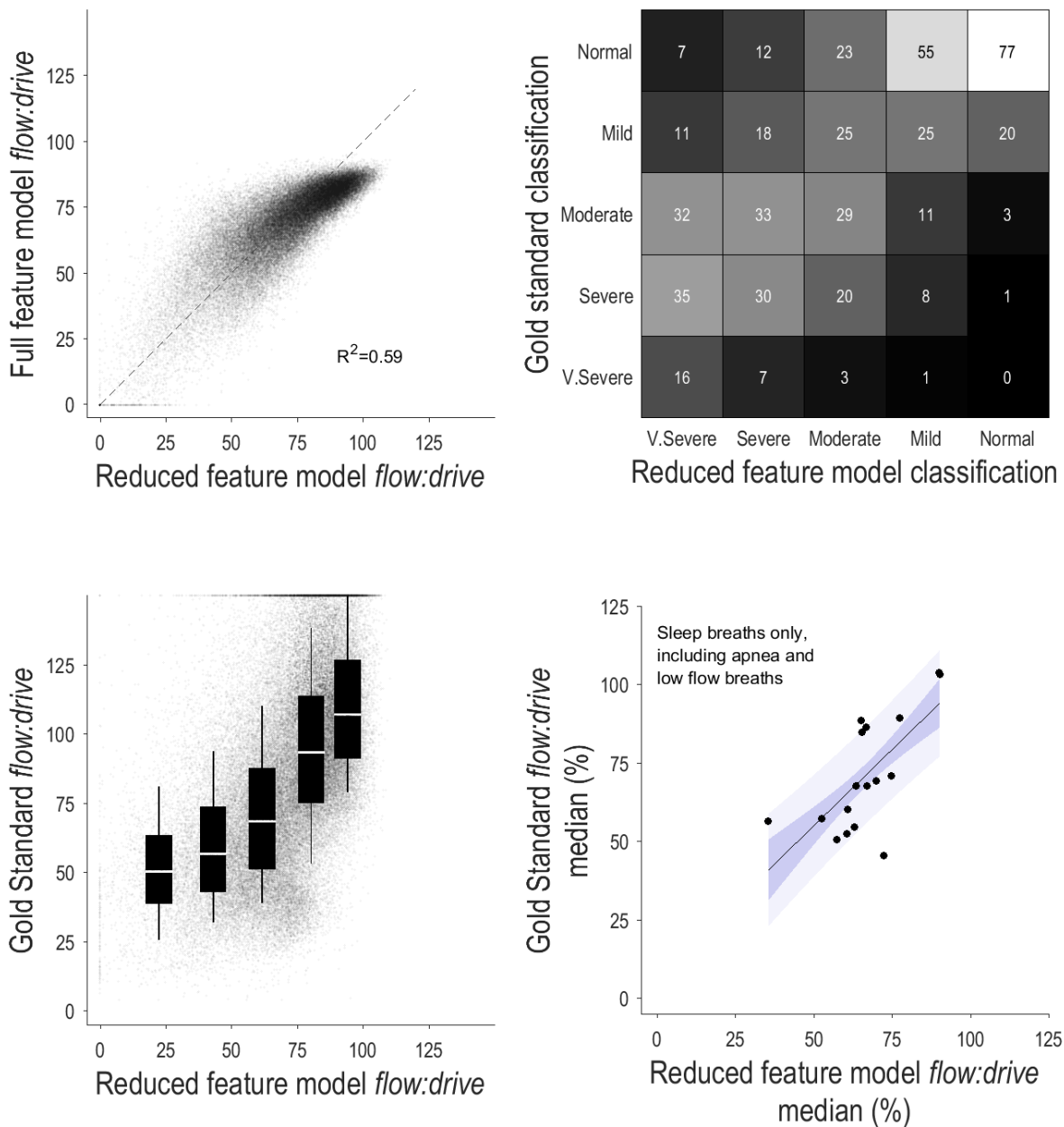
**Figure S6.** Reduced feature model performance, using *nasal pressure features*. **(Top Left)** The association between the reduced feature model predicted *flow:drive* values and the full 25 feature model predicted *flow:drive* values is moderate ($R^2$=0.59). **(Top Right)** Predictive performance confusion matrix for each severity classification, with thresholds being >90% Normal, 70-90% Mild, 50-70% Moderate, 30-50% Severe, <30% Very Severe (V.Severe). Each column sums to 100%, and indicates the fraction of predicted breaths in each class that were correctly classified. On average, the classification prediction was exact in 35.2% of breaths, and within one severity class in 76.4% of breaths. **(Bottom Left)** Scatter plot showing a strong association between reduced feature model predicted *flow:drive* and gold-standard *flow:drive* values. The box plot overlay shows summary statistics (box and central line show IQR and median respectively, whiskers show 10th and 90th percentiles) for breaths within each severity classification. **(Bottom Right)** Scatter plot showing the novel patient level metric, median *flow:drive* (during sleep, including apnoea breaths). A very strong association exists between reduced feature model predicted and gold-standard patient median *flow:drive* during sleep. ($R^2$, coefficient of determination).

**External validation**

We examined 29 baseline sleep studies as part of a separate investigation (NCT02489591) in which pneumotachograph airflow was measured via a sealed nasal mask. Participants details: 19M:10F, age $= 49\pm11$ years, BMI $= 32 \pm 7$ kg/m$^2$, neck circumference $= 40 \pm 5$ cm, AHI $= 45 \pm 28$ events/hr (range $= 2$ to 105 events/hr). Each study was scored carefully for clinically-relevant respiratory events (30% reduction in flow in association with either 3% desaturation or arousal) and EEG arousal start and end times were carefully scored (>3 seconds with no upper limit). Breaths were automatically labelled as likely "normal" or likely "obstructed" as follows: Breaths within the margins of a scored arousal that had a level of ventilation above the local 3 min average were considered likely "normal". Breaths within the margins of scored obstructive hypopnoea with a level of ventilation at least 30% below the local average were considered likely "obstructed". In total, we identified 9183 "normal" (arousal) breaths and 7544 "obstructed" (hypopnoea) breaths.

We estimated *flow:drive* values by applying the final 25 feature final model presented above, and examined the discriminative capacity of our method to separate "normal" versus "obstructed" breaths. A threshold of *flow:drive* < 70% (moderate-to-severe airflow obstruction) was used for a binary classification. We observed a positive predictive value of 88% and negative predictive value of 85% (Figure S7). Alternatively, use of the 5-feature model yielded similar results, with a positive predictive value of 88% and negative predictive value of 84% (not shown).
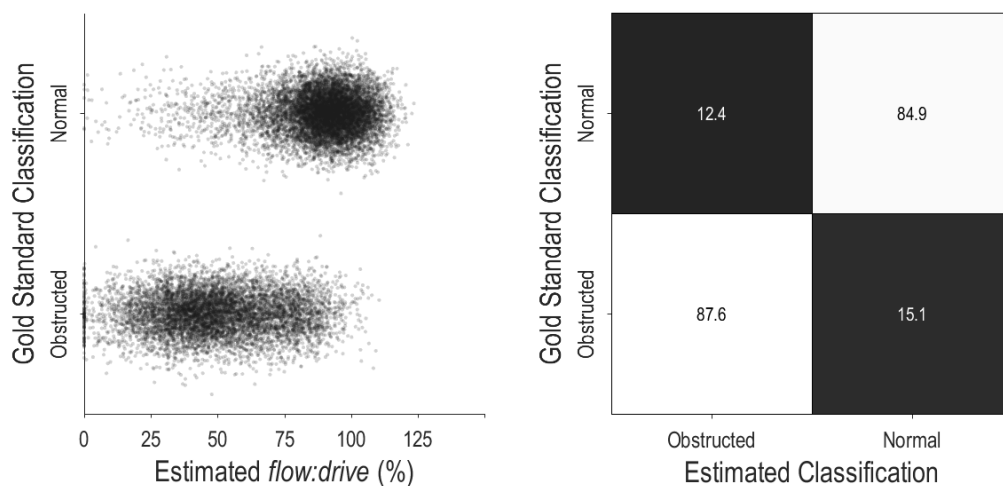


**Figure S7.** Classification performance using the 25 feature final model, with flow shape feature-terms derived from pneumotachograph flow in an alternate dataset. *Left:* Scatter plot showing the probability of a breath being "normal" (i.e. in arousal with larger than average flow) or "obstructed" (i.e. obstructive hypopnoea with <70% of normal flow). *Right:* Performance matrix. Each column sums to 100%, and as such can be used to quickly assess the fraction of breaths correctly classified. The values within each division of the confusion matrix show the proportion of total breaths. Positive predictive value is 88%. Negative predictive value = 85%.

**Feature pre-screening with external data**

As mentioned above, we also tested whether pre-screening features using this separate dataset might have improved the final model predictive value (potentially by early elimination of features that were of limited independent value in the determination of airflow obstruction). First, 165 feature terms were calculated (81/85 with "original" timing, and 84/85 with "transition" timing); multivariable *logistic* regression with backwards elimination was used to identify the 50 best feature terms (including timing variants) that discriminated between "normal" (arousal) breaths and "obstructed" (hypopnoea) breaths as defined above. This logistic regression model had positive predictive value of 89% and negative predictive value of 89% (cross-validated performance).

We then repeated the main flow shape analysis (Table S3, Figures 3 and 5) starting with pre-screened feature list (50 instead of 165), calculating the 3 transforms (square-root, untransformed, squared; 150 instead of 495), and then removing features with $R^2$ (pneumotach versus nasal pressure) <0.5 (leaving 92 instead of 295). Model performance at a breath level was similar with versus without pre-screening: For pneumotach analysis, $R^2 = 0.58$ under both conditions. For nasal pressure analysis, $R^2 = 0.43$ and 0.48 respectively. Thus there was no evidence to support the utility of the feature pre-screening approach described.

# Assessing Central versus Obstructive Pathophysiology: Future Directions

Strictly speaking, *flow:drive* indicates the magnitude of pharyngeal obstruction. Out of context with the changes in flow during respiratory events, *flow:drive* alone provides insufficient information to strictly determine a) the magnitude of central drive during events ($Y = \text{flow} \div \textit{flow:drive}$), and b) whether drive is rising or falling during hypopneas. Example analysis showing two patients with significantly different flow and drive patterns, which can be inferred from the estimated *flow:drive* (flow shapes), are shown in Figure S8.
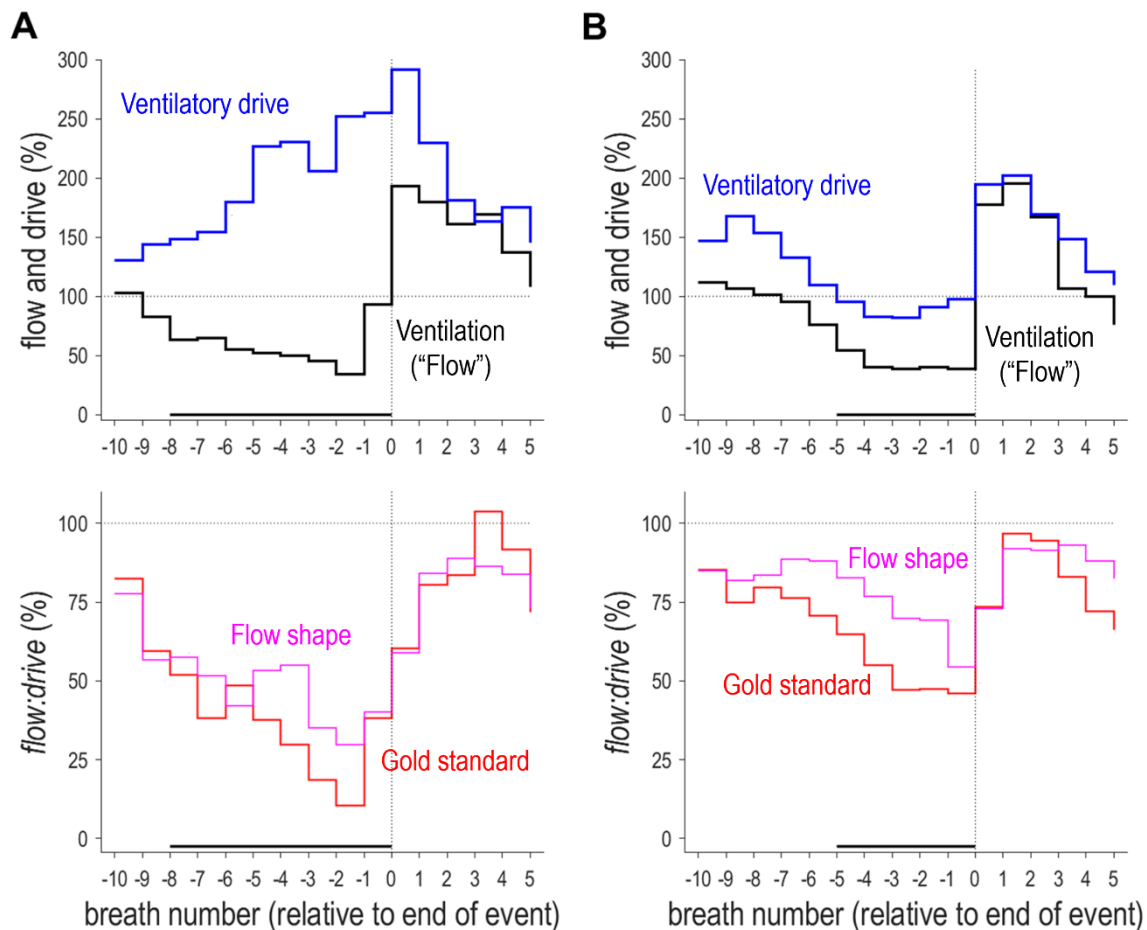


**Figure S8.** Ensemble-averaged hypopnea data in two patients illustrating evolving flow, drive, and obstruction across breaths. **(A)** The first patient (AHI=39 events/hr) exhibits increasing drive in response to falling flow throughout the hypopnea (horizontal bar, 8 breaths; top traces). Here, a progressively rising drive can be inferred from the observation that *flow:drive* falls by more than flow (bottom traces). **(B)** The second patient (AHI=80) exhibits a reduction in drive concurrent with the loss of flow; drive briefly falls marginally below the eupneic level. Here, a progressively falling drive can be inferred from the observation that *flow:drive* falls by less than flow. Drive and flow also change in parallel (positively associated); one may interpret that the fall in drive is facilitating the event itself. Ensemble averages were calculated for all available scored hypopneas in both patients; median data are shown for each breath. Ventilatory drive data are based on calibrated diaphragm EMG.

## Supplemental References

1.      Montserrat JM, Farre R, Ballester E, Felez MA, Pasto M, Navajas D. Evaluation of nasal prongs for estimating nasal flow. *American journal of respiratory and critical care medicine* 1997: 155(1): 211-215.
2.      Farre R, Rigau J, Montserrat JM, Ballester E, Navajas D. Relevance of linearizing nasal prongs for assessing hypopneas and flow limitation during sleep. *American journal of respiratory and critical care medicine* 2001: 163(2): 494-497.
3.      Terrill PI, Edwards BA, Nemati S, Butler JP, Owens RL, Eckert DJ, White DP, Malhotra A, Wellman A, Sands SA. Quantifying the ventilatory control contribution to sleep apnoea using polysomnography. *Eur Respir J* 2015: 45(2): 408-418.
4.      Sands SA, Edwards BA, Terrill PI, Taranto-Montemurro L, Azarbarzin A, Marques M, Hess LB, White DP, Wellman A. Phenotyping Pharyngeal Pathophysiology using Polysomnography in Patients with Obstructive Sleep Apnea. *American journal of respiratory and critical care medicine* 2018: 197(9): 1187-1197.
5.      Sands SA, Terrill PI, Edwards BA, Taranto Montemurro L, Azarbarzin A, Marques M, de Melo CM, Loring SH, Butler JP, White DP, Wellman A. Quantifying the Arousal Threshold Using Polysomnography in Obstructive Sleep Apnea. *Sleep* 2018: 41(1).
6.      Mooney AM, Abounasr KK, Rapoport DM, Ayappa I. Relative prolongation of inspiratory time predicts high versus low resistance categorization of hypopneas. *Journal of clinical sleep medicine : JCSM : official publication of the American Academy of Sleep Medicine* 2012: 8(2): 177-185.
7.      Mann DL, Edwards BA, Joosten SA, Hamilton GS, Landry S, Sands SA, Wilson SJ, Terrill PI. The relationship between partial upper-airway obstruction and inter-breath transition period during sleep. *Respiratory physiology & neurobiology* 2017: 244: 32-40.
8.      Milic-Emili J, Grunstein MM. Drive and timing components of ventilation. *Chest* 1976: 70(1 Suppl): 131-133.
9.      Azarbarzin A, Marques M, Sands SA, Op de Beeck S, Genta PR, Taranto-Montemurro L, de Melo CM, Messineo L, Vanderveken OM, White DP, Wellman A. Predicting epiglottic collapse in patients with obstructive sleep apnoea. *Eur Respir J* 2017: 50(3).
10.     Teschler H, Berthon-Jones M, Thompson AB, Henkel A, Henry J, Konietzko N. Automated continuous positive airway pressure titration for obstructive sleep apnea syndrome. *American journal of respiratory and critical care medicine* 1996: 154(3 Pt 1): 734-740.
11.     Camassa A, Franciosini A, Sands SA, Zhi YX, Yadollahi A, Bianchi AM, Wellman A, Redline S, Azabarzin A, Mariani S. Validating an Algorithm for Automatic Scoring of Inspiratory Flow Limitation within a Range of Recording Settings. *IEEE/40th Annual Conference of the IEEE Engineering in Medicine and Biology Society* 2018.
12.     Clark SA, Wilson CR, Satoh M, Pegelow D, Dempsey JA. Assessment of inspiratory flow limitation invasively and noninvasively during sleep. *American journal of respiratory and critical care medicine* 1998: 158(3): 713-722.
13.     Genta PR, Sands SA, Butler JP, Loring SH, Katz ES, Demko BG, Kezirian EJ, White DP, Wellman A. Airflow Shape Is Associated With the Pharyngeal Structure Causing OSA. *Chest* 2017: 152(3): 537-546.
14.     Zhi YX, Vena D, Popovic MR, Bradley TD, Yadollahi A. Detecting inspiratory flow limitation with temporal features of nasal airflow. *Sleep Med* 2018: 48: 70-78.
15.     Azarbarzin A, Sands SA, Marques M, Genta PR, Taranto-Montemurro L, Messineo L, White DP, Wellman A. Palatal prolapse as a signature of expiratory flow limitation and inspiratory palatal collapse in patients with obstructive sleep apnoea. *Eur Respir J* 2018: 51(2).
16.     Reich O, Brown K, Bates JH. Breathing patterns in infants and children under halothane anesthesia: effect of dose and CO2. *Journal of applied physiology* 1994: 76(1): 79-85.
17.     Schneider H, Krishnan V, Pichard LE, Patil SP, Smith PL, Schwartz AR. Inspiratory duty cycle responses to flow limitation predict nocturnal hypoventilation. *Eur Respir J* 2009: 33(5): 1068-1076.

18.    Martin RJ, Okken A, Katona PG, Klaus MH. Effect of lung volume on expiratory time in the newborn infant. *Journal of applied physiology: respiratory, environmental and exercise physiology* 1978: 45(1): 18-23.

19.    Carlsen KH, Lodrup Carlsen KC. Tidal breathing analysis and response to salbutamol in awake young children with and without asthma. *Eur Respir J* 1994: 7(12): 2154-2159.

20.    Beydon N, Davis SD, Lombardi E, Allen JL, Arets HG, Aurora P, Bisgaard H, Davis GM, Ducharme FM, Eigen H, Gappa M, Gaultier C, Gustafsson PM, Hall GL, Hantos Z, Healy MJ, Jones MH, Klug B, Lodrup Carlsen KC, McKenzie SA, Marchal F, Mayer OH, Merkus PJ, Morris MG, Oostveen E, Pillow JJ, Seddon PC, Silverman M, Sly PD, Stocks J, Tepper RS, Vilozni D, Wilson NM, American Thoracic Society/European Respiratory Society Working Group on I, Young Children Pulmonary Function T. An official American Thoracic Society/European Respiratory Society statement: pulmonary function testing in preschool children. *American journal of respiratory and critical care medicine* 2007: 175(12): 1304-1345.

21.    Morgenstern C, Schwaibold M, Randerath W, Bolz A, Jane R. Comparison of upper airway respiratory resistance measurements with the esophageal pressure/airflow relationship during sleep. *Conference proceedings : Annual International Conference of the IEEE Engineering in Medicine and Biology Society IEEE Engineering in Medicine and Biology Society Conference* 2011: 2011: 3205-3208.

22.    Miller MR, Pedersen OF, Quanjer PH. The rise and dwell time for peak expiratory flow in patients with and without airflow limitation. *American journal of respiratory and critical care medicine* 1998: 158(1): 23-27.

23.    Burdon JG, Pain MC. Maximal mid-inspiratory to maximal mid-expiratory flow rate ratio in upper airway obstruction. *The Medical journal of Australia* 1980: 1(5): 218-220.

24.    Series F, Marc I. Accuracy of breath-by-breath analysis of flow-volume loop in identifying sleep-induced flow-limited breathing cycles in sleep apnoea-hypopnoea syndrome. *Clinical science* 1995: 88(6): 707-712.

25.    van der Ent CK, van der Grinten CP, Meessen NE, Luijendijk SC, Mulder PG, Bogaard JM. Time to peak tidal expiratory flow and the neuromuscular control of expiration. *Eur Respir J* 1998: 12(3): 646-652.

26.    Morris MJ, Madgwick RG, Collyer I, Denby F, Lane DJ. Analysis of expiratory tidal flow patterns as a diagnostic tool in airflow obstruction. *Eur Respir J* 1998: 12(5): 1113-1117.

27.    Tamisier R, Pepin JL, Wuyam B, Deschaux C, Levy P. Expiratory changes in pressure: flow ratio during sleep in patients with sleep-disordered breathing. *Sleep* 2004: 27(2): 240-248.

28.    Sankri-Tarbichi AG, Rowley JA, Badr MS. Expiratory pharyngeal narrowing during central hypocapnic hypopnea. *American journal of respiratory and critical care medicine* 2009: 179(4): 313-319.